

Water Film Drainage between a Very Viscous Oil Drop and a Mica Surface

Tianzi Bai, Rogerio Manica[✉], and Bo Liu[✉]

Department of Chemical and Materials Engineering, University of Alberta, Edmonton, Canada T6G 1H9

Evert Klaseboer[✉]

Institute of High Performance Computing, 1 Fusionopolis Way, Singapore 138632

Zhenghe Xu

*Department of Chemical and Materials Engineering, University of Alberta, Edmonton, Canada T6G 1H9
and Department of Materials Science and Engineering, Southern University of Science and Technology,
Shenzhen 518055, China*

Qingxia Liu^{✉*}

*Department of Chemical and Materials Engineering, University of Alberta, Edmonton, Canada T6G 1H9
and College of New Materials and New Energies, Shenzhen Technology University, Shenzhen 518118, China*



(Received 27 April 2021; accepted 25 August 2021; published 17 September 2021)

We investigate thin film drainage between a viscous oil drop and a mica surface, clearly illustrating the competing effects of Laplace pressure and viscous normal stress (τ_v) in the drop. τ_v dominates the initial stage of drainage, leading to dimple formation (h_d) at a smaller critical thickness with an increase in the drop viscosity (the dimple is the inversion of curvature of the drop in the film region). Surface forces and interfacial tension control the last stage of film drainage. A scaling analysis shows that h_d is a function of the drop size R and the capillary numbers of the film (Ca_f) and drop (Ca_d), which we estimate by $h_d = 0.5R\sqrt{Ca_f/(1+2Ca_d)}$. This equation clearly indicates that the drop viscosity needs to be considered when $Ca_d > 0.1$. These results have implications for industrial systems where very viscous liquids are involved, for example, in 3D printing and heavy oil extraction process.

DOI: [10.1103/PhysRevLett.127.124503](https://doi.org/10.1103/PhysRevLett.127.124503)

The film drainage process between an oil drop or air bubble and solid surfaces is of great importance in many industrial applications, including heavy oil extraction and 3D printing. This is particularly true for heavy oils or fluids of ultrahigh viscosity, which is a crucial property of bitumen and some polymers applied in 3D printing. As a drop approaches a solid surface in an aqueous phase, an inversion of the curvature of the aqueous film appears at some stage, which is called “dimple formation” [1]. Such a dimple may lead to the capture of small water drops and air bubbles, which is detrimental for 3D printing technology [2,3]. The Stokes–Reynolds–Young–Laplace model [4] is well established to predict film drainage between an oil drop of relative low viscosity (< 0.1 Pa s) and a solid surface. A wide range of capillary numbers of the water film ($Ca_f = \mu_w V/\gamma$, where μ_w is the viscosity of water, V is the approach velocity, and γ is the oil–water interfacial tension) ranging from $Ca_f = 10^{-8}$ to 10^{-2} has been investigated and a universal relation for the height of initial dimple formation has been established, which can be expressed as $h_d \sim R\sqrt{Ca_f}$, where R is the radius of the drop [5–8]. Increasing the approach velocity and decreasing the oil–water or air–water interfacial tension [6,8] was found to

affect the height of the dimple occurrence. However, the effect of the capillary number of the oil drop ($Ca_d = \mu_o V/\gamma$, with μ_o being the viscosity of oil) on the film drainage process received little attention. Langley *et al.* [9,10] studied the impact of an ultraviscous drop on solid and water surfaces in air. The initial dimple was scaled by an empirical impact parameter that resulted in a relationship of $h_d \sim \mu_o^{-1/9}$. Some axisymmetric models for the coalescence between two ultraviscous drops or a drop against a solid surface have also been developed. The tangential immobile boundary condition was shown to be applicable at the oil–water interface for the systems with high oil–water viscosity ratio (μ_o/μ_w) [11]. In addition, some numerical models were developed to calculate the drop profile and lubrication force under the assumption of constant approach velocity or constant interaction force [12,13]. However, the viscosity ratio considered in those models was still not high enough for the viscous stress to play a role in the drop deformation. Such subject therefore remains to be addressed.

In this Letter, we report the drainage of the thin liquid water film between an oil drop of ultrahigh viscosity and a mica surface using high-speed interferometric images that

can provide quantitative information throughout the whole film drainage process. The capillary number of the oil drop Ca_d in this study ranged from 10^{-8} to 30 using drops of viscosity ranging from ~ 0.001 to ~ 100 Pa s. The capillary number of the aqueous film Ca_f ranged from 10^{-7} to 10^{-4} . The height of dimple occurrence was precisely obtained by analyzing the interference fringes. Using scaling arguments, we derived an analytical formula that can accurately predict the dimple height over a wide range of drop capillary numbers, which requires one to take the viscous normal stress inside the oil drop into consideration. We observed a substantially different film drainage process, which was likely caused by the competition between the Laplace pressure and the viscous normal stress across the surface.

The drainage of the aqueous film between highly viscous drops and a surface was studied using the dynamic force apparatus (DFA). A schematic of the DFA is shown in Fig. 1(a) [8]. An oil drop with radius $R = 1.05 \pm 0.01$ mm was generated at the end of a capillary tube. The mica surface was freshly cleaved before its use to obtain a hydrophilic surface with the water contact angle of $\sim 0^\circ$. The initial distance between the oil drop and the mica surface was set at $350 \mu\text{m}$, which was monitored and controlled by a side view camera. By using the motorized actuator, the oil drop was driven toward to mica surface for $500 \mu\text{m}$, which we termed “displacement,” so that interaction happens, and the oil drop will form a dimple, as seen in the schematic of Fig. 1(b). The drop approach velocities were selected from 0.1 to 10 mm/s.

The interference fringes were observed by an inverted Axiovert 100 Carl Zeiss microscope and were recorded by a high-speed video camera (Photron SA4,

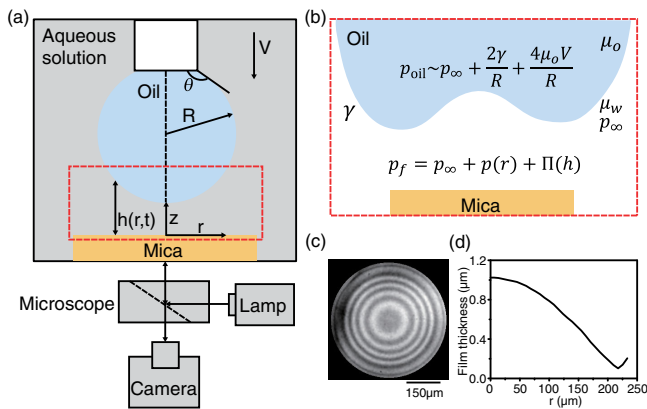


FIG. 1. (a) Schematic of the dynamic force apparatus. An oil drop with radius $R = 1.05 \pm 0.01$ mm was generated at the end of a capillary. The drop was driven toward the hydrophilic mica surface by a motor. (b) Thin film region corresponding to the red square in (a). (c) A snapshot of the interference fringes (green channel) obtained between an oil drop and a mica surface ($\mu_o = 25.8$ Pa s, $V = 1.06$ mm/s) in 0.1 mM SDS solution. (d) Axisymmetric film thickness profile obtained from (c).

60–500 000 frames/s). Figure 1(c) shows an example of the interference fringes between a drop of 25.8 Pa s viscosity interacting with the mica surface. The film thickness as a function of radial coordinate was obtained by analyzing the fringes using the method adopted by Scheludko and Platikanowa [14,15].

The evolution of the film thickness between the oil drop of 0.001 Pa s viscosity and the surface is shown in Fig. 2(a). It is noted that the viscosity of oils used in this study was

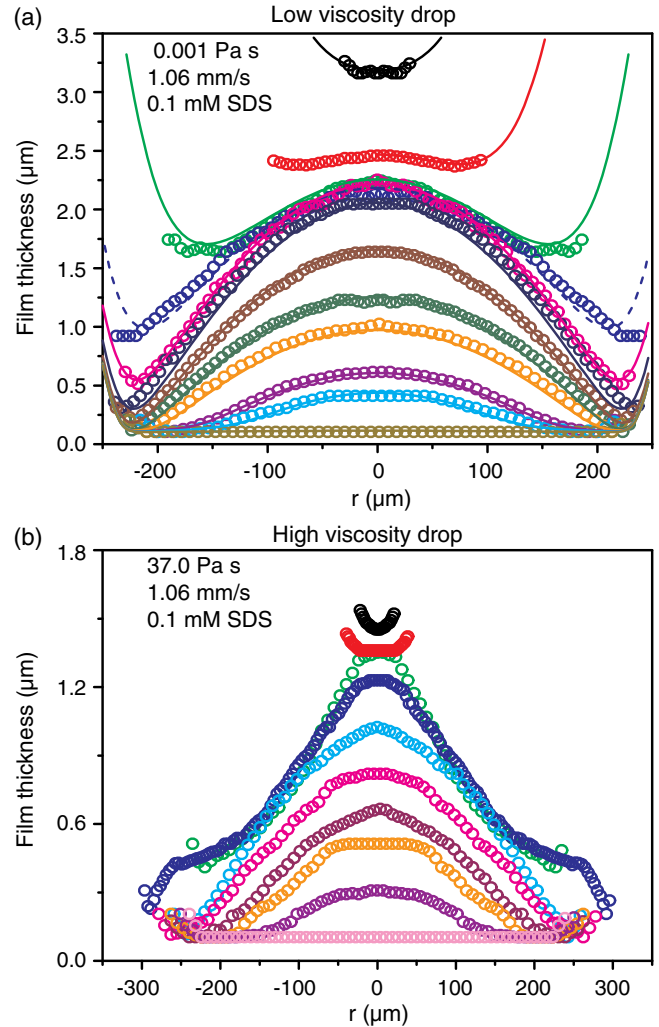


FIG. 2. (a) Comparison between the experimental results (points) and the theoretical model (lines) for the film evolution of an oil drop of 0.001 Pa s viscosity interacting with a mica surface in 0.1 mM SDS aqueous solution at the approach velocity of 1.06 mm/s ($Ca_d = 10^{-5}$). The measured times of the profiles from top to bottom are $-0.015, 0.018, 0.085, 0.218, 0.55, 2.12, 9.07, 31.8, 66.4, 153.5, 211.9,$ and 331.7 s. The dashed line indicates when the oil drop stopped moving. (b) Film drainage process using an oil drop of 37.0 Pa s viscosity in 0.1 mM SDS aqueous solution at the approach velocity of 1.06 mm/s ($Ca_d = 0.8$). The measured times of the profiles from top to bottom are $-0.001, 0, 0.067, 0.618, 19.7, 97.1, 144.5, 211.0, 318.1,$ and 391.6 s. Drop stopped moving at 0.26 s.

measured by the hybrid rheometer and remained constant for shear rates range from 0.001 to 10 s^{-1} . Sodium dodecyl sulfate (SDS) was added into the solution to fully immobilize the oil-water interface for the low-viscosity oil drop and to adjust the oil-water interfacial tension by changing its concentration [16–18]. The time $t = 0$ is defined as the moment of dimple formation. In this case, the drop forms a dimple at a height of around 2570 nm . As the film drains, the film thickness at the center first decreases to and then remains at around 2243 nm [$t = 0.085 \text{ s}$ in Fig. 2(a)]. The dimple becomes increasingly more pronounced as the film thickness at the barrier rim keeps decreasing. With the drive being stopped at $t = 0.218 \text{ s}$, the film thickness at the center first slightly increases, which is called the “center bounce” phenomenon [6,8]. After that, the water film continues to drain with the film width remaining almost constant.

The film drainage process for an oil drop of high viscosity interacting with the solid surface exhibits different features. Figure 2(b) shows an example of the film profiles between a silicone oil drop of 37.0 Pa s viscosity interacting with the mica surface. A distinctly different film drainage process is described as follows.

During the approach of the drop to the solid surface, the dimple formed at a lower height, as shown in Fig. 2(b). The height of dimple formation decreased further when increasing the oil viscosity [Fig. 3(a)], which is consistent with impacting highly viscous drops in air [9]. Such a feature cannot be explained by the silicone oil-water interfacial tension, as it barely changes with the increasing viscosity [19]. At a lower approach velocity (0.1 mm/s) for oil drops of a lower interfacial tension (in 1 mM SDS solution), the initial dimple height also decreased with increasing oil viscosity. (See Supplemental Material for detailed definition of dimple height, film drainage process of other selected conditions, and physical properties of oil [20].)

After dimple formation, the film height at the center of the film remains almost stationary despite the decrease in the minimum film height at the barrier rim. However, a pointy-shaped dimple was formed, as shown in the green curve ($t = 0.067 \text{ s}$) in Fig. 3(b). After the drop stopped moving at $t = 0.26 \text{ s}$, the water drained out, resulting in a decrease of center film thickness followed by expansion of the barrier rim. A film shape of a changing curvature formed at the same time, as shown in the dark blue curve ($t = 0.618 \text{ s}$) in Fig. 3(b). The change in film curvature at a radius of around $250 \mu\text{m}$ was also found in impacting drop experiments [28,29]. Finally, the radius of the barrier rim decreased and the pointy center gradually disappeared, as shown in the light blue curve ($t = 19.7 \text{ s}$) in Fig. 3(b).

Eventually, the water drained out under the Laplace pressure, with the final thickness controlled by the repulsive disjoining pressure due to the negatively charged drop and mica surfaces [30–33]. A stable film of about 100 nm was formed.

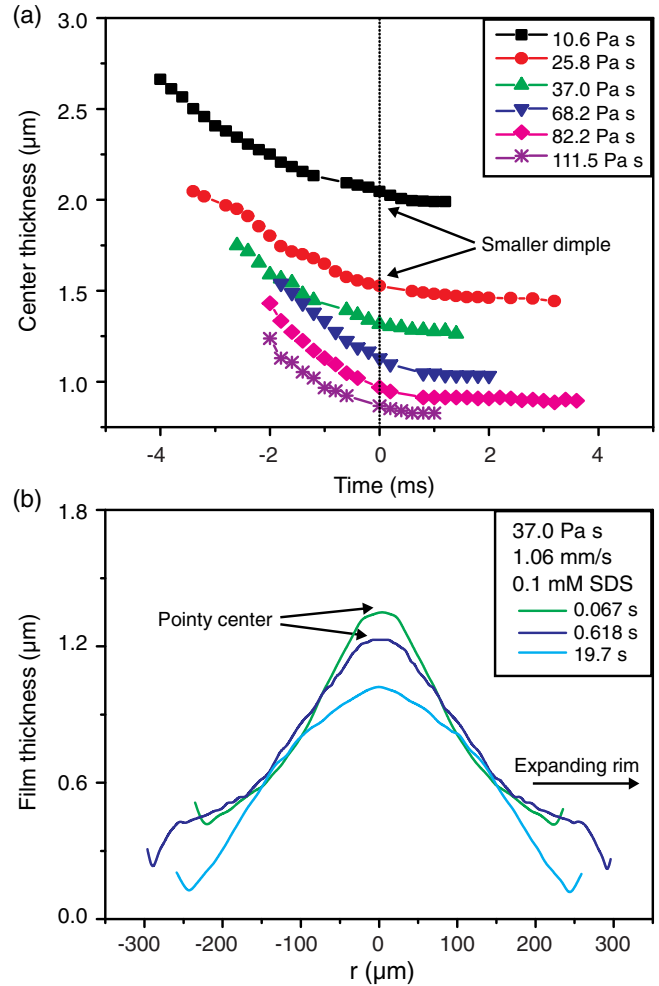


FIG. 3. (a) Film thickness at the center $h(0, t)$ as a function of time for oil drops of different viscosity in 0.1 mM SDS solution at an approach velocity of 1.06 mm/s . (b) Selected drop shape profiles of an oil drop of 37.0 Pa s viscosity from Fig. 2(b) in 0.1 mM SDS aqueous solution at the approach velocity of 1.06 mm/s at times 0.067 , 0.618 , and 19.7 s .

We applied a scaling method to explain the decreasing height of dimple formation as a function of drop viscosity. In this model, we used the Stokes equation to describe the dynamics of the viscous drop [34]. The detailed derivation of equations can be found in the Supplemental Material [20]. By applying a simplified scaling analysis while considering the vertical velocity at the center point of the drop $v_{\text{center}} \sim V$ and radial dimension $r \sim R$ inside the oil drop, we estimated the contribution of the normal stress τ_v from the viscosity of the drop by

$$\tau_v \simeq \frac{2\mu_o V}{R}. \quad (1)$$

Considering the contributions to the film pressure by the Laplace pressure and the pressure in the bulk solution (p_∞), we approximate the pressure p_{oil} along the bottom of the oil drop [see also Fig. 1(b)] by

$$p_{\text{oil}} \approx 2 \left(\frac{\gamma}{R} + \frac{2\mu_o V}{R} \right) + p_{\infty}. \quad (2)$$

The difference between the pressure inside the oil drop and in the thin film ($p_{\text{oil}} - p_f$), which drives the lubrication flow, is

$$p_{\text{oil}} - p_f = \frac{2\gamma}{R} + \frac{4\mu_o V}{R} - p(r) - \Pi(h), \quad (3)$$

where $p(r)$ is the excess hydrodynamic pressure in the water film and $\Pi(h)$ is the disjoining pressure due to surface forces. We define the characteristic pressure p_0 from Eqs. (2) and (3) as having contributions from the Laplace pressure and the viscous normal stress given by

$$p_0 = \frac{\gamma}{R} + \frac{2\mu_o V}{R} = \frac{\gamma}{R} (1 + 2Ca_d). \quad (4)$$

The thin film drainage is described by Reynolds lubrication theory. Here, we assume tangentially immobile boundary conditions at oil-water interfaces because the viscosity of an oil drop is much higher than the surrounding aqueous solution [11]. For the low-viscosity oil, the surfactant in the solution can also give rise to a immobile boundary condition [16–18],

$$\frac{\partial h}{\partial t} = \frac{1}{12\mu_w r} \frac{\partial}{\partial r} \left(rh^3 \frac{\partial p}{\partial r} \right). \quad (5)$$

Based on the radial dimension $r_0 = \sqrt{Rh_0}$ [5,35] and $h_0/t_0 = V$, Eq. (5) provides the following relation between all nondimensional parameters

$$V = \frac{1}{\mu_w} \frac{h_0^3 p_0}{Rh_0}. \quad (6)$$

Eliminating p_0 with Eq. (4) results in the characteristic film thickness

$$h_0 = R \sqrt{\frac{Ca_f}{1 + 2Ca_d}}. \quad (7)$$

We note that the nondimensional thickness of dimple formation $h'_d = h_d/h_0$ for the interaction between two drops or between a drop and a solid surface can vary from 0.4 to 0.7 if the drops or bubbles are pinned to a solid surface, depending on the pinning angle and the fluid-fluid boundary conditions [4,36,37]. Since the angle that the oil or bubble makes at the end of the capillary in our experiment is around 140° with immobile boundary conditions, the film thickness at which the dimple appears is around $h'_d \sim 0.5$ [8]. Thus, a general relation that holds at both low and high oil viscosity can be expressed as

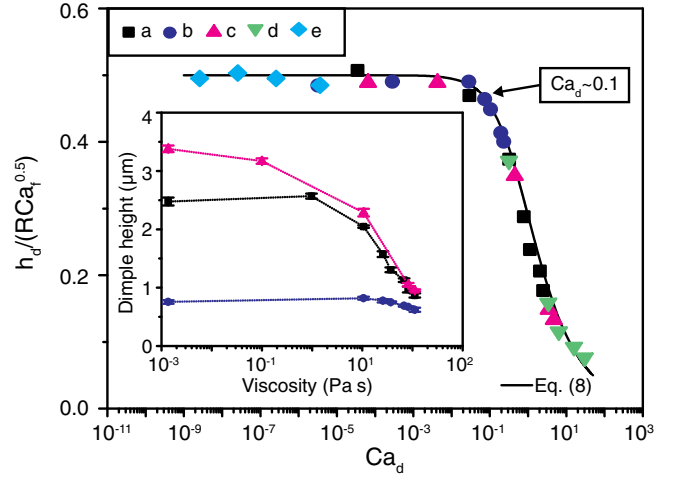


FIG. 4. Height of initial dimple formation for oil drops or bubbles interacting with a hydrophilic solid surface in water, as a function of Ca_d as compared with the theoretical curve of Eq. (8) (line). The five different cases are (a) $V = 1.06$ mm/s in 0.1 mM SDS solution, $\mu_o = 0.001$ –111.5 Pa s; (b) $V = 0.1$ mm/s in 0.1 mM SDS solution, $\mu_o = 0.001$ –111.5 Pa s; (c) $V = 1.06$ mm/s in 1 mM SDS solution, $\mu_o = 0.001$ –111.5 Pa s; (d) $\mu_o = 111.5$ Pa s in 0.1 mM SDS solution, $V = 0.1$ –10 mm/s; (e) bubble interacting with silica in water. The data of the dimple height for bubble interacting with hydrophilic silica surface in water (e) is from Ref. [8]. The result of the theoretical calculation fit well with the results from corresponding experiments. The transition occurred at Ca_d around 0.1. Inset: the height of initial dimple formation as a function of oil viscosity (same legend).

$$h_d = 0.5h_0 = 0.5R \sqrt{\frac{Ca_f}{1 + 2Ca_d}}. \quad (8)$$

Figure 4 shows the comparison between the experimental and calculated scaled dimple height using Eq. (8) as a function of Ca_d . The film thickness at dimple formation is scaled using the length scales ($R\sqrt{Ca_f}$) typical of current system. The inset shows the dimple height as a function of oil viscosity. The prediction based on Eq. (8) is in good agreement with the results of our experiments. It is worth noting that obtaining the exact value of the dimple height is extremely difficult, if not impossible, although a very high frame rate (5000 frames/s) was used in this study. The reported dimple heights are an average of the center height of 3–5 frames of two videos and the height of the initial dimple formation varied within a range of around 50 nm.

The master curve in Fig. 4 predicts the thickness of initial dimple formation for the drop capillary number Ca_d ranging from 10^{-8} to 30, including different approach velocities, interfacial tension, and drop viscosity. For a system of comparable viscosity of the drop to that of bulk solutions, i.e., $Ca_d < 0.1$, the viscous contribution to the normal stress inside the oil drop is small as compared with the Laplace pressure; that is, $Ca_d \ll 1$. The pressure

difference across the oil-water interface is mainly due to the Laplace pressure. The scaling $h'_d = 0.5$ and $h_d \sim R\sqrt{\text{Ca}_f}$ holds for both our study and the results of a bubble in water against a silica surface [4,8]. When the oil viscosity is larger (in other words, increasing Ca_d), p_{oil} increases due to the larger viscous normal stress $2\mu_o V/R$. Increasing pressure difference across the oil-water interface, which has a similar effect as increasing the effective interfacial tension, renders the drop more difficult to deform, thus resulting in a decrease in h_d . When Ca_d is greater than 0.1, as shown in Fig. 4, the viscous effect inside the drop cannot be neglected. However, the model can only qualitatively predict the full drainage process as the expression of the viscous normal stress is based on scaling argument.

In summary, by considering the viscous normal stress inside the oil drop, we showed that the competition between the Laplace pressure and viscous normal stress inside the drop was responsible for a significantly reduced height of initial dimple formation. After the drive of the drop stopped, the viscous normal stress became negligible, resulting in the film drainage being controlled by the disjoining pressure. The initial deformation characteristics for the oil interacting with a solid surface in a SDS aqueous solutions was well captured by an analytical formula [Eq. (8)], which holds for a wide range of drop capillary numbers. At low drop capillary number, the capillary force was found to be dominant and the universal scaling $h_d \sim R\sqrt{\text{Ca}_f}$ described the drop deformation. When the capillary number of the oil drop $\text{Ca}_d > 0.1$, the viscosity of the oil drop needed to be taken into consideration and the drop capillary number became a dominant factor. Our systematic study verified that the viscous normal stress inside the very viscous oil drop, which leads to a higher effective interfacial tension, is the fundamental reason for decreasing the drop deformation.

The financial support for this project from the Natural Sciences and Engineering Research Council of Canada (NSERC) and Syncrude Canada, Ltd. is very much appreciated.

* qingxia2@ualberta.ca

- [1] R. S. Allan, G. Charles, and S. Mason, The approach of gas bubbles to a gas/liquid interface, *J. Colloid Sci.* **16**, 150 (1961).
- [2] S. Thoroddsen, T. Etoh, K. Takehara, N. Ootsuka, and Y. Hatsuki, The air bubble entrapped under a drop impacting on a solid surface, *J. Fluid Mech.* **545**, 203 (2005).
- [3] E. G. Gordeev, A. S. Galushko, and V. P. Ananikov, Improvement of quality of 3d printed objects by elimination of microscopic structural defects in fused deposition modeling, *PLoS One* **13**, e0198370 (2018).
- [4] D. Y. Chan, E. Klaseboer, and R. Manica, Theory of non-equilibrium force measurements involving deformable drops and bubbles, *Adv. Colloid Interface Sci.* **165**, 70 (2011).
- [5] E. Klaseboer, J. P. Chevaillier, C. Gourdon, and O. Masbernat, Film drainage between colliding drops at constant approach velocity: Experiments and modeling, *J. Colloid Interface Sci.* **229**, 274 (2000).
- [6] J. N. Connor and R. G. Horn, The influence of surface forces on thin film drainage between a fluid drop and a flat solid, *Faraday Discuss.* **123**, 193 (2003).
- [7] R. Manica, M. H. Hendrix, R. Gupta, E. Klaseboer, C.-D. Ohl, and D. Y. Chan, Effects of hydrodynamic film boundary conditions on bubble-wall impact, *Soft Matter* **9**, 9755 (2013).
- [8] X. Zhang, R. Manica, P. Tchoukov, Q. Liu, and Z. Xu, Effect of approach velocity on thin liquid film drainage between an air bubble and a flat solid surface, *J. Phys. Chem. C* **121**, 5573 (2017).
- [9] K. Langley, E. Li, and S. T. Thoroddsen, Impact of ultraviscous drops: Air-film gliding and extreme wetting, *J. Fluid Mech.* **813**, 647 (2017).
- [10] K. Langley and S. T. Thoroddsen, Gliding on a layer of air: Impact of a large-viscosity drop on a liquid film, *J. Fluid Mech.* **878** (2019).
- [11] S. G. Yiantsios and R. H. Davis, On the buoyancy-driven motion of a drop towards a rigid surface or a deformable interface, *J. Fluid Mech.* **217**, 547 (1990).
- [12] I. Bazhlekov, A. Chesters, and F. Van de Vosse, The effect of the dispersed to continuous-phase viscosity ratio on film drainage between interacting drops, *Int. J. Multiphase Flow* **26**, 445 (2000).
- [13] R. H. Davis, J. A. Schonberg, and J. M. Rallison, The lubrication force between two viscous drops, *Phys. Fluids* **1**, 77 (1989).
- [14] A. Scheludko and D. Platikanowa, Untersuchung dunner flüssiger schichten auf quecksilber, *Kolloid Z.* **175**, 150 (1961).
- [15] L. Parkinson and J. Ralston, The interaction between a very small rising bubble and a hydrophilic titania surface, *J. Phys. Chem. C* **114**, 2273 (2010).
- [16] B. Liu, R. Manica, Q. Liu, E. Klaseboer, Z. Xu, and G. Xie, Coalescence of Bubbles with Mobile Interfaces in Water, *Phys. Rev. Lett.* **122**, 194501 (2019).
- [17] Y. Amarouchene, G. Cristobal, and H. Kellay, Noncoalescing Drops, *Phys. Rev. Lett.* **87**, 206104 (2001).
- [18] D. Langevin, Bubble coalescence in pure liquids and in surfactant solutions, *Curr. Opin. Colloid Interface Science* **20**, 92 (2015).
- [19] A. El-Hamouz, Effect of surfactant concentration and operating temperature on the drop size distribution of silicon oil water dispersion, *J. Dispersion Sci. Technol.* **28**, 797 (2007).
- [20] See Supplemental Material at <http://link.aps.org/supplemental/10.1103/PhysRevLett.127.124503> for details on bubble generation, interferometry method, model description and prediction, and video showing (1) details of dimple height extraction, (2) drive function of drop movement, (3) initial film drainage stage for different cases, (4) overall film drainage process of selected conditions, (5) physical properties of different oils, (6) model description, and (7) comparison between model and experimental

- data. Video also shows dimple formation, which includes Refs. [21–27].
- [21] X. Zhang, P. Tchoukov, R. Manica, L. Wang, Q. Liu, and Z. Xu, Simultaneous measurement of dynamic force and spatial thin film thickness between deformable and solid surfaces by integrated thin liquid film force apparatus, *Soft Matter* **12**, 9105 (2016).
- [22] F. Peters and D. Arabali, Interfacial tension between oil and water measured with a modified contour method, *Colloids Surf.* **426**, 1 (2013).
- [23] A. Kanellopoulos and M. Owen, Adsorption of sodium dodecyl sulphate at the silicone fluid/water interface, *Trans. Faraday Soc.* **67**, 3127 (1971).
- [24] A. R. White and T. Ward, Surface remobilization of buoyancy-driven surfactant-laden drops at low Reynolds and capillary numbers, *AIChE J.* **65**, 294 (2019).
- [25] M. Zaucha, Z. Adamczyk, and J. Barbasz, Zeta potential of particle bilayers on mica: A streaming potential study, *J. Colloid Interface Sci.* **360**, 195 (2011).
- [26] A. M. Djerdjev and J. K. Beattie, Electroacoustic and ultrasonic attenuation measurements of droplet size and ζ -potential of alkane-in-water emulsions: Effects of oil solubility and composition, *Phys. Chem. Chem. Phys.* **10**, 4843 (2008).
- [27] E. Freer, H. Wong, and C. Radke, Oscillating drop/bubble tensiometry: Effect of viscous forces on the measurement of interfacial tension, *J. Colloid Interface Sci.* **282**, 128 (2005).
- [28] J. de Ruiter, D. van den Ende, and F. Mugele, Air cushioning in droplet impact. II. Experimental characterization of the air film evolution, *Phys. Fluids* **27**, 012105 (2015).
- [29] R. C. A. van der Veen, T. Tran, D. Lohse, and C. Sun, Direct measurements of air layer profiles under impacting droplets using high-speed color interferometry, *Phys. Rev. E* **85**, 026315 (2012).
- [30] Y. Gu and D. Li, Electric charge on small silicone oil droplets dispersed in ionic surfactant solutions, *Colloids Surf.* **139**, 213 (1998).
- [31] S. Nishimura, H. Tateyama, K. Tsunematsu, and K. Jinnai, Zeta potential measurement of muscovite mica basal plane-aqueous solution interface by means of plane interface technique, *J. Colloid Interface Sci.* **152**, 359 (1992).
- [32] E. J. W. Verwey, J. T. G. Overbeek, and K. Van Nes, *Theory of the Stability of Lyophobic Colloids: The Interaction of Sol Particles Having an Electric Double Layer* (Elsevier Publishing Company, New York, 1948).
- [33] J. N. Israelachvili, *Intermolecular and Surface Forces* (Academic Press, New York, 2011).
- [34] C. K. Batchelor and G. Batchelor, *An Introduction to Fluid Dynamics* (Cambridge University Press, Cambridge, England, 2000).
- [35] Y. Wang, C. Dhong, and J. Frechette, Out-of-Contact Elastohydrodynamic Deformation Due to Lubrication Forces, *Phys. Rev. Lett.* **115**, 248302 (2015).
- [36] E. Klaseboer, J.-P. Chevallier, A. Maté, O. Masbernat, and C. Gourdon, Model and experiments of a drop impinging on an immersed wall, *Phys. Fluids* **13**, 45 (2001).
- [37] M. Shahalami, L. Wang, C. Wu, J. H. Masliyah, Z. Xu, and D. Y. Chan, Measurement and modeling on hydrodynamic forces and deformation of an air bubble approaching a solid sphere in liquids, *Adv. Colloid Interface Sci.* **217**, 31 (2015).